

## Error-resistant single-qubit gates with trapped ions

N. Timoney,<sup>1</sup> V. Elman,<sup>1</sup> S. Glaser,<sup>2</sup> C. Weiss,<sup>1</sup> M. Johanning,<sup>1</sup> W. Neuhauser,<sup>3</sup> and Chr. Wunderlich<sup>1</sup>

<sup>1</sup>*Fachbereich Physik, Universität Siegen, 57068 Siegen, Germany*

<sup>2</sup>*Department Chemie, Technische Universität München, Lichtenbergstrasse 4, 85747 Garching, Germany*

<sup>3</sup>*Institut für Laser-Physik, Universität Hamburg, Luruper Chaussee 149, 22761 Hamburg, Germany*

(Received 13 December 2006; revised manuscript received 19 March 2008; published 30 May 2008)

Coherent operations with individual trapped Yb<sup>+</sup> ions are demonstrated that are robust against variations in experimental parameters and intrinsically indeterministic system parameters. In particular, pulses developed using optimal control theory are demonstrated with trapped ions. Their performance as a function of error parameters is systematically investigated and compared to composite pulses. Such pulses are basic building blocks for single and multiqubit quantum gates.

DOI: [10.1103/PhysRevA.77.052334](https://doi.org/10.1103/PhysRevA.77.052334)

PACS number(s): 03.67.Lx, 42.50.Ct

### I. INTRODUCTION

In order to experimentally implement a device capable of performing fault-tolerant universal quantum computation (QC), quantum gate operations involving one or multiple qubits have to be carried out with demanding high accuracy (e.g., Refs. [1,2]). According to recent theoretical investigations, the experimentally required accuracy of quantum gates for fault-tolerant universal quantum computation no longer seems daunting or even prohibitive [2]. But still, the desired error probability per gate (EPG) should be as small as possible in order to keep the experimental overhead necessary for quantum computation within a feasible limit. Thus a low error probability is prerequisite for scalable fault-tolerant QC.

Any quantum algorithm can be decomposed into a sequence of unitary operations applied to individual qubits (single-qubit gate) and conditional quantum dynamics with at least two qubits [3]. Multiqubit gates (involving two or more qubits) are synthesized by applying a sequence of elementary unitary operations on a collection of qubits. Each of these elementary operations is often similar, or identical, to what is needed for single-qubit gates, and therefore each operation has to be implemented with an error probability well below the tolerable EPG characterizing the full gate operation.

If electrostatically trapped ions are used as qubits, then a unitary operation amounts to letting ions interact with electromagnetic radiation with prescribed frequency, phase, amplitude, and duration of interaction in order to implement quantum gates. Recently, impressive experimental progress was demonstrated in entangling up to eight ions, and performing two-qubit quantum gates [4–6]. Architectures allowing for scalable QC with trapped ions have been proposed (e.g., [7]), and building blocks necessary for achieving this ambitious goal are currently being investigated using various types of ions.

The error budget, for instance, of the geometrical phase gate demonstrated in Ref. [6] is dominated by the frequency and amplitude uncertainty of the laser light field. These errors are also responsible for a part of the EPG of the controlled-NOT gate reported in Ref. [5]. If an “ion spin molecule,” that is, trapped ions coupled via a long range spin

interaction, is to be used for quantum information processing, then the exact transition frequency of a particular ionic qubit depends on the internal state of other ions [8]. Therefore, here too, it is important to have quantum gates at hand that are insensitive to the detuning of the radiation driving the qubit transition.

Here, we demonstrate single qubit gates and rotations on the Bloch sphere that serve as building blocks for gates with trapped ions that are robust against experimental imperfections over a wide range of parameters. In particular it is shown that errors caused by an inaccurate setting of either frequency, amplitude, or duration of the driving field, or of a combination of these errors are tolerable (in terms of a desired accuracy of quantum gates) when a suitable sequence of radiation pulses is applied instead of, for instance, a single rectangular  $\pi$  pulse. Thus an essential prerequisite for scalable quantum computation with trapped ions is demonstrated.

### II. OPTIMAL CONTROL THEORY PULSES

Optimal control methods make it possible to design pulses that are not only robust with respect to frequency detunings but simultaneously also with respect to the amplitude of the irradiation [9–12]. In general, robust single qubit gates should work for arbitrary input states. Such pulses are called class A [or unitary rotation (UR)] pulses. In Ref. [13], it was demonstrated that robust UR pulse with nutation angle  $\theta$  can be constructed in a straight forward way from robust class B [or point-to-point (PP)] pulses with angle  $\theta/2$ . For example, a  $\pi/2$  PP excitation pulse designed to rotate a vector from the  $z$  axis to the  $-y$  axis can be used to construct a  $\pi$  UR pulse effecting a  $\pi$  rotation around the  $x$  axis for any initial state. The composite  $\pi$  UR pulse consists of the phase-inverted  $\pi/2$  PP pulse (with the algebraic signs of all phases inverted), followed by the time-reversed  $\pi/2$  PP pulse [13]. Hence, PP pulses are not only interesting for applications where the initial (or final) spin state is known (e.g., for initial preparation of superpositions or readout), but also serve as basic building blocks for the construction of robust UR pulses [12,13]. Here, we demonstrate the performance of optimal control-based shaped PP pulses [9,10] for  $\pi/2$  and  $\pi$  rotations of trapped ions. In addition, composite UR pulses

are implemented that are either designed to tackle off-resonance errors, or designed to tackle pulse amplitude errors [14]. In nuclear magnetic resonance quantum logic experiments, conventionally optimized shaped pulses have frequently been used, for example, to implement frequency selective rotations [15].

### III. EXPERIMENTAL SYSTEM: TRAPPED Yb<sup>+</sup> IONS

The two level quantum mechanical system used as qubit is realized on the  $|0\rangle \equiv S_{1/2}(F=0) \leftrightarrow S_{1/2}(F=1, m_F=0) \equiv |1\rangle$  transition in a single  $^{171}\text{Yb}^+$  ion. The Bohr frequency of the ion is denoted  $\omega_0$ . The ion itself is confined in a miniature Paul trap (diameter of 2 mm) and driven by microwave radiation with frequency  $\omega$  close to  $2\pi \times 12.6$  GHz and Rabi frequency  $\Omega \approx 2\pi \times 10$  kHz. The time evolution of the qubit is virtually free of decoherence, that is, transversal and longitudinal relaxation rates are negligible, and is determined in a rotating frame after the rotating wave approximation, by the semiclassical Hamiltonian  $H = \frac{\hbar}{2}\delta\sigma_z + \frac{\hbar}{2}\Omega(\sigma_+e^{-i\Phi} + \sigma_-e^{i\Phi})$ . Here,  $\sigma_{\pm}$  are the atomic raising and lowering operators,  $\sigma_z$  is a Pauli matrix, and  $\delta \equiv \omega_0 - \omega$  is the detuning of the applied radiation with respect to the atomic transition. Imperfect preparation of the  $|0\rangle$  state by optical pumping limits the purity of the initially prepared state such that the initial density matrix (before coherent interaction with microwave radiation) is given by  $\rho_i = a_1|1\rangle\langle 1| + a_0|0\rangle\langle 0|$  with typical values  $a_1 = 0.1$  and  $a_0 = 0.9$ . Imperfect detection efficiency also limits the upper bound of the fidelity measured.

The ion is produced from its neutral precursor by photo-ionization using a diode laser operating near 399 nm. Laser light near 369 nm driving resonantly the  $S_{1/2}F=1 \leftrightarrow P_{1/2}F=0$  transition in Yb<sup>+</sup> is supplied by a frequency doubled Ti:sapphire laser, and serves for cooling and state selectively detecting the ion. A diode laser delivers light near 935 nm and drives the  $D_{3/2} \leftrightarrow [3/2]_{1/2}$  transition to avoid optical pumping into the metastable  $D_{3/2}$  state during the cooling and detection periods (for details see Ref. [16]). To quantify errors in the detuning we will use the scaled detuning  $f = \delta/\Omega$ , whereas errors in pulse area shall be represented by  $g = \Delta\theta/\theta$ , where  $\Delta\theta = \theta' - \theta$  with the desired pulse area  $\theta = \int_0^T \Omega dt$  and the actual pulse area  $\theta'$  when  $T$  or  $\Omega$  are not set perfectly.

The fidelity of the qubit state  $|\theta_m, \phi_m\rangle \equiv \cos(\theta_m/2)|0\rangle + e^{i\phi_m}\sin(\theta_m/2)|1\rangle$  that is obtained after applying a microwave pulse is given by  $F = |\langle \theta, \phi | \theta_m, \phi_m \rangle|^2$  with  $|\theta, \phi\rangle$  being the state that would be obtained, if the pulse were perfect. Thus, for a  $\theta = \pi$  pulse the fidelity is given by  $F_{\pi} = |\sin(\theta_m/2)|^2$ . Impure initial preparation ( $a_1 > 0$ ) limits the maximum fidelity that can be obtained with a  $\pi$  pulse to  $F_{\pi} = a_0 - a_1$ .

In order to determine the fidelity of the state obtained after a gate that is supposed to leave the qubit with a well defined phase  $\phi$  (e.g., a  $\pi/2$  pulse), the phase  $\phi_m$  needs to be determined in addition to  $\theta_m$ . A Ramsey-type experiment allows for measuring both angles: First an ideal Ramsey sequence is carried out (i.e., two successive ideal  $\pi/2$  pulses with varying phase  $\Phi$  of the second pulse) yielding interference fringes in the population of state  $|1\rangle$ ,  $a_1$  as a function of

$\Phi$ . Then, the first  $\pi/2$  pulse is replaced by a possibly non-ideal pulse sequence leaving the qubit in state  $|\theta_m, \phi_m\rangle$ , and again interference fringes are recorded. Now the population  $a_1(\Phi)$  detected in state  $|1\rangle$  is given by Eq. (1), and from a fit of the data using

$$a_1(\Phi) = 1/2[1 + \sin(\theta_m)\cos(\phi_m + \Phi)] \quad (1)$$

one obtains  $\theta_m$  and  $\phi_m$ .

The expected performance of the optimal control-based, composite, and rectangular pulses, respectively, is simulated by numerical simulation of the time evolution of the density matrix of a two level system. The simulated results shown below assume ideal initial preparation and final read-out (i.e., 100% efficiency of both processes) of the qubit without longitudinal or transverse damping. The simulations also provide the possibility to visualize the time evolution of the qubit's state on the Bloch sphere.

### IV. MEASUREMENT TECHNIQUE

The basic measurement sequence (labeled sequence A) for determining the fidelity as a function of  $f$  and  $g$  of a shaped pulse that ideally gives a rotation with  $\theta = \pi$  is as follows: (i) A single ion is prepared in the  $|0\rangle$  state by optical pumping through illumination with 369 nm light for 20 ms. (ii) A microwave shaped pulse with controlled error, that is, known values of  $f$  and  $g$ , is applied. (iii) Again, the ion is illuminated for 5 ms with 369 nm light for state-selective detection. (iv) The ion is laser cooled by applying microwave and laser radiation simultaneously.

This sequence comprising steps (i)–(iv) is then repeated (sequence B), except that in step (ii), for direct comparison, the shaped pulse is replaced by a rectangular pulse that would give  $\theta = \pi$ , if  $f=0=g$ . Then, (i)–(iv) is repeated again (sequence C) with an ideal (i.e.,  $f=0=g$ )  $\pi/2$  rectangular pulse in step (ii) (that is supposed to yield equal probabilities for detecting state  $|0\rangle$  and  $|1\rangle$ , respectively) to check whether the experimental setup performs as it should (in particular the state-selective detection). Finally, (i)–(iv) is repeated a fourth time (sequence D) leaving out step (ii) in order to monitor the initial preparation in terms of the coefficient  $a_0$ . Typically, the full procedure (sequences A–D) outlined here is repeated 700 times for a given pair of  $f$  and  $g$  values.

When measuring the performance of shaped pulses and pulse sequences that ideally yield a rotation of  $\theta = \pi/2$  and, for instance,  $\phi = -\pi/2$ , then the basic sequence A' is as described above, except that in step (ii) two ideal ( $f=0=g$ )  $\pi/2$  pulses are applied, the second one with variable phase  $\Phi$  (this yields Ramsey fringes as a reference). Then, sequence B' is performed by replacing the first  $\pi/2$  pulse in step (ii) by a shaped pulse with controlled error. Sequence C' is obtained by replacing the first  $\pi/2$  pulse in (ii) with a rectangular pulse subject to the same errors as the shaped pulse in B'. Sequences A'–C' are repeated 20 times while increasing the value of  $\Phi$  by  $2\pi/20$ . Then sequences C and D are appended and the complete procedure is repeated 50 times. As an example, Fig. 1 illustrates how angles  $\theta_m, \phi_m$  were determined for a specific pair of  $f$  and  $g$  values.

A completed measurement returns two grids of fidelities with the points on each grid defined by different values of  $f$

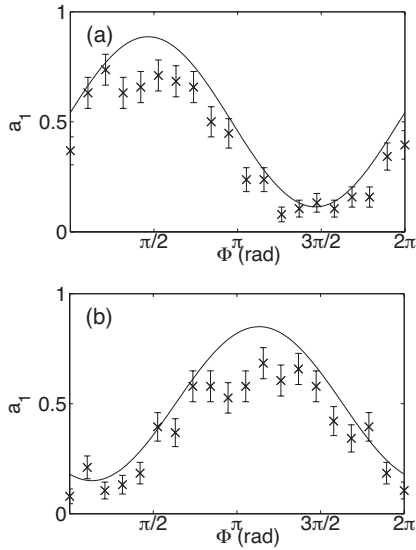


FIG. 1. (a) Ramsey interference fringes from sequence A' and (b) from sequence B' ( $f=-1$ ,  $g=0$ ). A fit (indicated by a solid line) of the experimental data using Eq. (1) gives  $\theta_m=3.92 \pm 0.05$ ,  $\phi_m=-0.418 \pm 0.11$  (see text).

and  $g$ . One grid corresponds to a simple pulse (obtained from sequences B or C'), that is, the amplitude as a function of time has a rectangular shape with the desired pulse area  $\theta = \Omega t$ . This pulse results in a perfect rotation by an angle  $\theta$  only for  $f=0$  and  $g=0$ . The second grid of fidelities corresponds to a shaped or composite pulse (obtained from sequence A or B'). In the experimental results shown below, crossing points between gridlines represent measurement points. The shaded areas are obtained by linear interpolation between points.

## V. OPTIMAL CONTROL-BASED PULSES: RESULTS

The optimal control-based pulses demonstrated here were designed for off-resonant errors described by  $-1 < f < 1$ , power variations up to  $\pm 40\%$ , Rabi frequency  $\Omega=2\pi \times 10$  kHz, and are made of  $0.5 \mu\text{s}$  steps. In each step, in general, amplitude and phase of the radiation is changed. As an example the time evolution of phase and amplitude of a pulse consisting of 645 individual steps is shown in Fig. 2 [10] (rotation of  $\theta=\pi/2$ ,  $\phi=-\pi/2$ ). A tabulated version of this pulse can be found in Ref. [17]. Also shown in Fig. 2 is the numerically simulated evolution of the qubit's state for scaled amplitude deviation  $g=0$  and scaled detuning  $f=-0.5$  on the surface of the Bloch sphere as a time trace starting at  $t=0$  on the south pole of the Bloch sphere.

The experimentally determined fidelity  $F$  of this shaped pulse as a function of  $f$  and  $g$  is displayed in Fig. 3. For reference, Fig. 3 also shows the experimental fidelity obtained from a simple rectangular  $\pi/2$  gate for the same parameter range.

To allow for a better quantitative comparison between the two types of pulses, we determine the parameter values for which the scaled fidelity  $F/F_m$  is larger than a reference value. Here,  $F_m$  denotes the maximal experimental fidelity

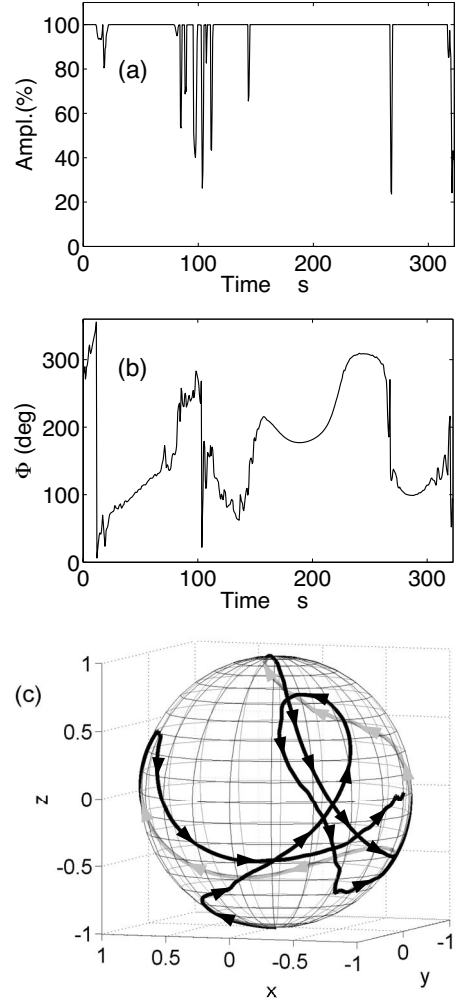


FIG. 2. (a) Relative amplitude and (b) phase of an optimal control-based  $\pi/2$  pulse consisting of 645 individual time steps [10] (available as supplementary online material) [17]. (c) shows the simulated time evolution of the pulse on the Bloch sphere, for  $g=0$  and  $f=-0.5$ . At  $t=0$  the state vector starts on the south pole of the Bloch sphere and reaches the desired state ( $\theta=\pi/2$ ,  $\phi=-\pi/2$ ) at the end of the pulse.

obtained for a given pulse. For  $f=0=g$  the shaped pulse yields the maximum fidelity  $F_m=0.900 \pm 0.014$ , and the values of  $f$  and  $g$  for which  $F/F_m > 0.90$  ( $F/F_m < 0.90$ ) is indicated in Fig. 3(a) by white (black) rectangles. This maximum value is maintained over a much wider parameter range than for the rectangular pulse [see Fig. 3(b) with  $F_m=0.899 \pm 0.041$ ], thus demonstrating the robustness of the shaped pulse against experimental errors and intrinsic imperfections.

In the right graph of Fig. 3, the results of simulations for the optimal control theory pulse depicted in Fig. 2 and the simple pulse are shown. The experimentally observed dependence of the fidelity on the parameters  $f$  and  $g$  is well reproduced by these numerical simulations up to a scaling factor (the latter is mainly due to experimentally imperfect initial preparation and detection of the qubit as outlined above).

Figure 4 displays the experimental fidelity obtained by using a shaped  $\pi$  pulse consisting of 445 steps with variable

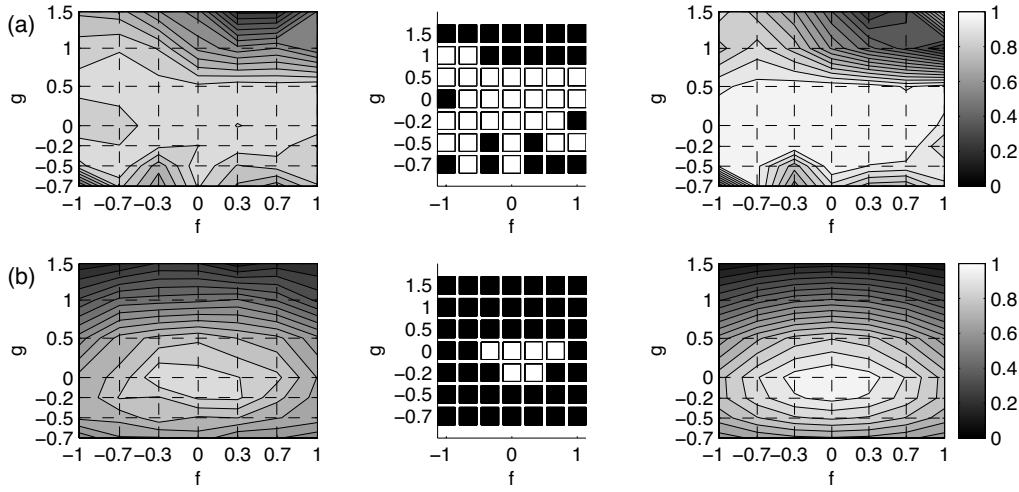


FIG. 3. (a) Experimental fidelity  $F$  for the optimal control-based ( $\theta=\frac{\pi}{2}$ ,  $\phi=-\frac{\pi}{2}$ ) pulse shown in Fig. 2 as a function of scaled detuning  $f$  and relative error in the nutation angle  $g$ . The average statistical error of the measured points is  $\sigma_{\text{av}}=0.023$ . The center graphic is based on the same data and a white (black) rectangle indicates  $F/F_m > 0.90$  ( $F/F_m < 0.90$ ) with the maximal fidelity  $F_m=0.900 \pm 0.014$ . Finally on the right graph the results of the simulation generated by the time evolution of the density matrix are shown. (b) Corresponding data for a rectangular  $\pi/2$  pulse ( $\sigma_{\text{av}}=0.035$ ,  $F_m=0.899 \pm 0.041$ ). Identical gray scales are used for plotting the experimental data (left column) and numerically simulated data (right column).

phase and amplitude subject to controlled errors. Again, a rectangular pulse serves as an experimental reference giving a maximum fidelity  $F_m=0.760 \pm 0.026$  for  $f=0=g$  that rapidly decreases for increasing  $|f|$  or  $|g|$ . The shaped pulse, in contrast, maintains the maximal possible fidelity over a wide range of parameters as is evident from Fig. 4.

In Fig. 5 the experimental results of another optimal control theory based  $\pi$  pulse are shown as an example. This pulse consisted of 835 steps. Again the maximum fidelity ( $F_m=0.790 \pm 0.035$ ) shown has been limited by the imperfect preparation and detection of the system.

The pulses whose experimental fidelity is displayed in Figs. 4 (445 steps) and 5 (835 steps), respectively, were developed to maximize the fidelity in a region with an offset

range of 20 kHz, that is  $-1 < f < 1$  with a Rabi frequency of 10 kHz, and a variation in the amplitude of the radiation driving the qubit of  $\pm 40\%$ , where each step is  $0.5 \mu\text{s}$  long and can be different in phase or in amplitude [10]. A tabulated version of both these pulses can be found in [17]. From comparing Figs. 4 and 5 it is evident that the longer pulse extends the region of parameter space where a high fidelity is obtained even further. An optimal control-based pulse can easily (and should) be adapted to a particular experimental situation (relevant range of errors in experimental parameters, sources of decoherence, relevant coherence times). Often a more restricted area of error resistance than shown in Fig. 5 is sufficient, and thus optimal control-based pulses can

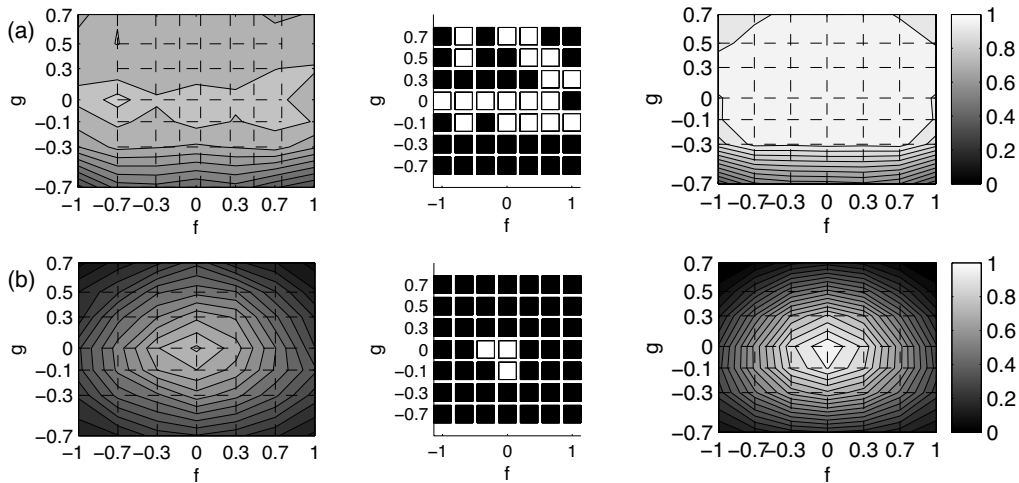


FIG. 4. (a) Experimental fidelity for an optimal control-based  $\theta=\pi$  pulse (445 steps) [17],  $\sigma_{\text{av}}=0.025$ ,  $F_m=0.821 \pm 0.027$ , white rectangles indicate  $F/F_m > 0.9$  and (b) for a rectangular  $\pi$  pulse ( $\sigma_{\text{av}}=0.018$ ,  $F_m=0.760 \pm 0.026$ ). The simulated results are shown in the right column for both the optimal control-based pulse and the rectangular pulse.

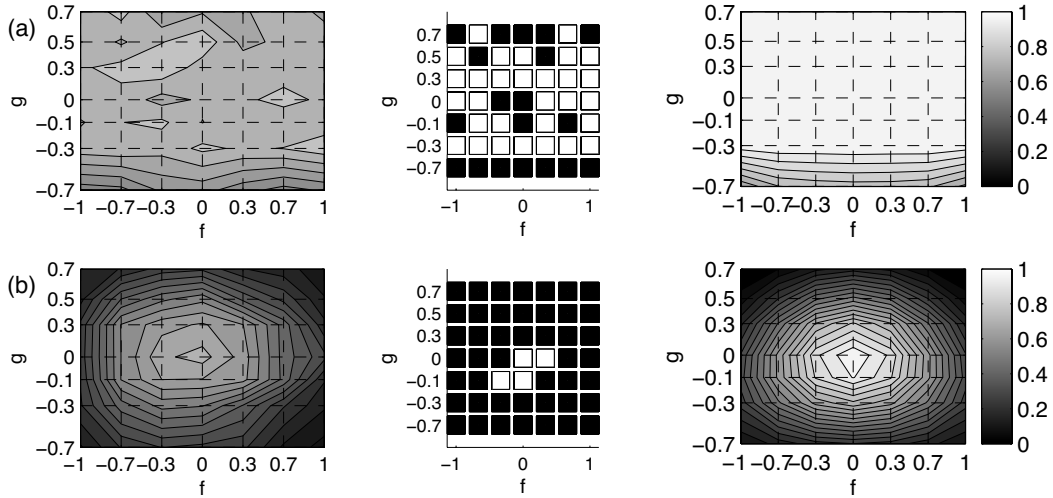


FIG. 5. (a) Experimental fidelity for an optimal control-based  $\theta=\pi$  pulse (835 steps) [17],  $\sigma_{av}=0.034$ ,  $F_m=0.790 \pm 0.035$ , white rectangles indicate  $F/F_m > 0.9$  and (b) for a rectangular  $\pi$  pulse ( $\sigma_{av}=0.024$ ,  $F_m=0.720 \pm 0.035$ ). The right column shows the simulated results of the optimal control-based pulse and the rectangular pulse.

be made considerably shorter and/or vary more smoothly in time than, for instance, shown in Fig. 2.

**VI. COMPOSITE PULSES: RESULTS**

Now, we compare the performance of these pulses to some composite pulses that have been devised to be effective against off-resonance, amplitude, and pulse length errors. The resulting fidelity grids were measured by sequentially performing the composite case and the simple case for each point on the grid, and then repeating 300 times. In terms of the previously used description, sequence A and sequence B are performed for each point on the grid, they are followed by C and D, then the complete measurement procedure is performed 300 times.

The composite pulse of type compensation for off-resonance with a pulse sequence (CORPSE) was derived

with the aim of combatting off-resonant errors [14]. It consists of three pulses where the first and the third pulses have equal phase values  $\Phi$  and the phase of the second pulse differs by  $\pi$ . The nutation angles of the three pulses making up a  $\pi$  composite pulse are  $420^\circ$ ,  $300^\circ$ ,  $60^\circ$ . Indeed, as shown in Fig. 6(a) the CORPSE  $\pi$  pulse extends the experimentally determined range of detuning  $f$  over which a fidelity  $F/F_m > 0.96$  ( $F_m=0.839 \pm 0.038$ ) is maintained as compared to the rectangular pulse shown in Fig. 6(b). However, for compensating pulse area errors this pulse sequence is less effective as is also evident from Fig. 6.

Similarly a  $\pi/2$  pulse shown is the BB1 (broadband) composite pulse comprises a sequence  $W=180_{\Phi_1}-360_{\Phi_2}-180_{\Phi_3}$  [14]. When the desired rotation is  $R(\theta)$ , the complete rotation can be performed as  $R(\theta)-W$ ,  $W-R(\theta)$ , or  $(\theta/2)-W-R(\theta/2)$ . The measurement procedure follows the proce-

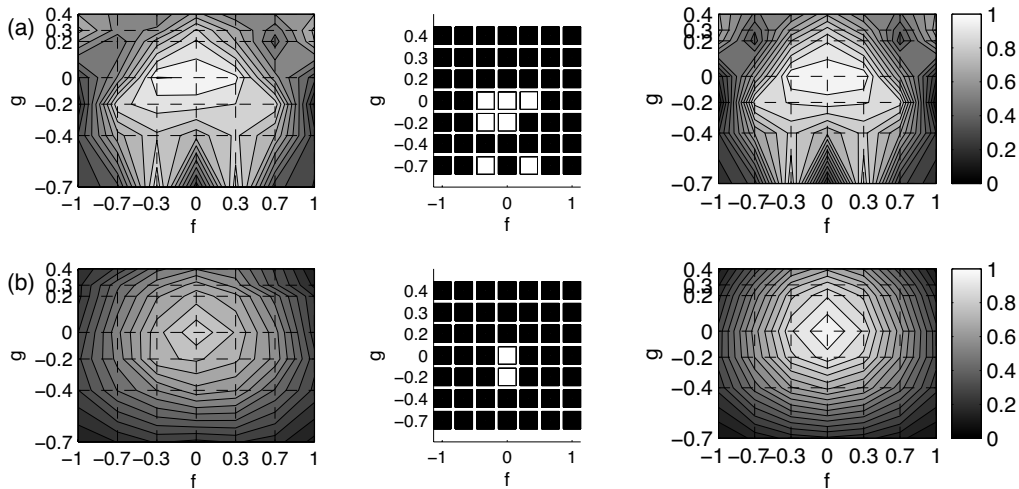


FIG. 6. (a) Experimental fidelity for a CORPSE-type composite pulse ( $\theta=\pi$ ,  $\sigma_{av}=0.030$ ,  $F_m=0.853 \pm 0.038$  white rectangles indicate  $F/F_m > 0.9$ ). The right column shows the simulated results using the same gray scale as the experimentally obtained fidelity. (b) Shows the same for the corresponding rectangular pulse ( $F_m=0.839 \pm 0.038$ ,  $\sigma_{av}=0.027$ ).

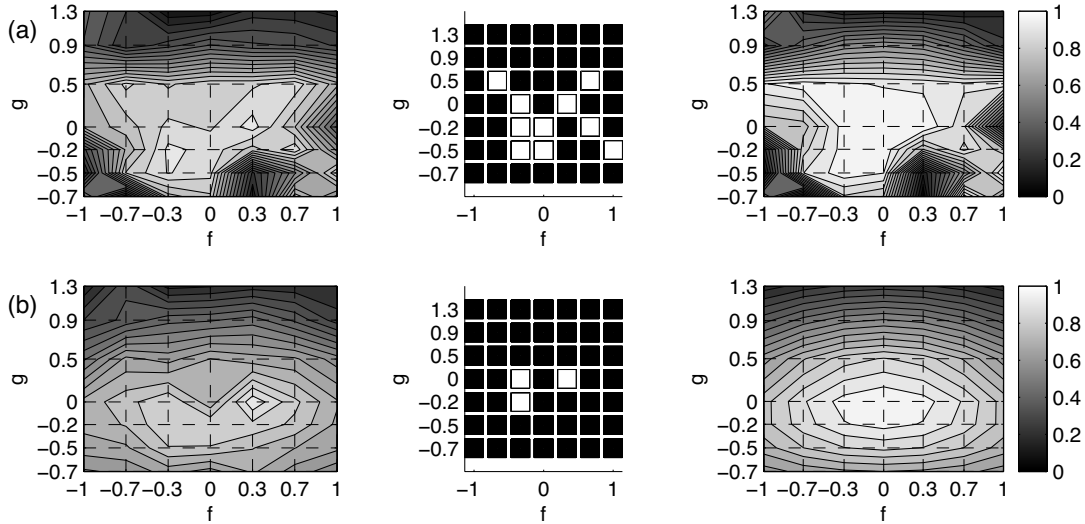


FIG. 7. Experimental fidelity for the BB1  $R(\frac{\theta}{2})-W-R(\frac{\theta}{2})$  sequence ( $\theta=\frac{\pi}{2}$ ,  $\phi=0$ ),  $F_m=0.924 \pm 0.008$ ,  $\sigma_{av}=0.023$ , white rectangles indicate  $F/F_m > 0.90$ , the simulated values are shown in the right column. (b) Shows the same for the corresponding rectangular pulse, where  $F_m=0.936 \pm 0.009$ ,  $\sigma_{av}=0.024$ .

procedure outlined above for the shaped  $\pi/2$  pulse. Shown in Fig. 7 are the results of using the BB1 composite pulse  $R(\theta/2) - W - R(\theta/2)$  with  $\theta = \pi/2$ . The experimental data show that BB1 is effective for compensation of errors in both detuning and pulse area. The parameter range over which error resistant pulses are effective is greater than that of a simple pulse but is more restricted than with the optimal control-based shaped pulse shown in Fig. 3.

A comparison of the performance of shaped pulses developed using optimal control theory with simple rectangular pulses or composite pulses reveals an evident advantage of these shaped pulses in terms of robustness against experimental errors and indeterministic system parameters, while the lengths of both types of pulses are comparable (here, with  $\Omega = 2\pi \times 10$  kHz, for instance, the pulse in Fig. 4 takes

223  $\mu\text{s}$  compared to 217  $\mu\text{s}$  for a CORPSE pulse of Fig. 6). Here, we demonstrate basic building blocks of unitary gates that are exemplary for optimal control-based pulses with trapped ions. We emphasize that such pulses can be made robust against variation in any desired range of the parameters  $f$  (detuning) and  $g$  (amplitude) as is shown in Refs. [10,13]. This will make shaped pulses based on optimal control theory an important tool in order to achieve quantum gates with trapped ions with low error probability and thus come a step closer to fault-tolerant quantum computing.

#### ACKNOWLEDGMENT

We acknowledge financial support from the European Union IP QAP.

- 
- [1] P. Aliferis, D. Gottesman, and J. Preskill, *Quantum Inf. Comput.* **6**, 97 (2006).  
 [2] E. Knill, *Nature (London)* **434**, 39 (2005).  
 [3] A. Barenco, C. H. Bennett, R. Cleve, D. P. DiVincenzo, N. Margolus, P. Shor, T. Sleator, J. A. Smolin, and H. Weinfurter, *Phys. Rev. A* **52**, 3457 (1995). For certain quantum computational tasks, gates that simultaneously act on more than two qubits have been shown to be more efficient than the use of two-qubit gates.  
 [4] D. Leibfried *et al.*, *Nature (London)* **438**, 639 (2005); H. Häffner *et al.*, *ibid.* **438**, 643 (2005); P. C. Haljan, P. J. Lee, K.-A. Brickman, M. Acton, L. Deslauriers, and C. Monroe, *Phys. Rev. A* **72**, 062316 (2005); J. P. Home *et al.*, *New J. Phys.* **8**, 188 (2006).  
 [5] F. Schmidt-Kaler *et al.*, *Nature (London)* **422**, 408 (2003).  
 [6] D. Leibfried *et al.*, *Nature (London)* **422**, 412 (2003).  
 [7] D. Kielpinski, C. Monroe, and D. J. Wineland, *Nature (London)* **417**, 709 (2002).  
 [8] C. Wunderlich, in *Laser Physics at the Limit* (Springer, Heidelberg, 2002), p. 261; F. Mintert and C. Wunderlich, *Phys. Rev. Lett.* **87**, 257904 (2001); D. Mc Hugh and J. Twamley, *Phys. Rev. A* **71**, 012315 (2005).  
 [9] T. E. Skinner *et al.*, *J. Magn. Reson.* **163**, 8 (2003).  
 [10] K. Kobzar *et al.*, *J. Magn. Reson.* **170**, 236 (2004).  
 [11] N. Khaneja *et al.*, *J. Magn. Reson.* **172**, 296 (2005).  
 [12] T. E. Skinner *et al.*, *J. Magn. Reson.* **179**, 241 (2006).  
 [13] B. Luy *et al.*, *J. Magn. Reson.* **176**, 179 (2005).  
 [14] H. K. Cummins, G. Llewellyn, and J. A. Jones, *Phys. Rev. A* **67**, 042308 (2003).  
 [15] For instance, J. A. Jones and M. Mosca, *J. Chem. Phys.* **109**, 1648 (1998); R. Marx, A. F. Fahmy, J. M. Myers, W. Bermel, and S. J. Glaser, *Phys. Rev. A* **62**, 012310 (2000); N. Boulant, K. Edmonds, J. Yang, M. A. Pravia, and D. G. Cory, *ibid.* **68**, 032305 (2003).

- [16] C. Wunderlich and C. Balzer, *Adv. At., Mol., Opt. Phys.* **49**, 293 (2003); C. Balzer, A. Braun, T. Hannemann, C. Paape, M. Ettl, W. Neuhauser, and C. Wunderlich, *Phys. Rev. A* **73**, 041407(R) (2006).
- [17] See EPAPS Document No. E-PLRAAN-77-150804 for tabulated step by step version of the optimal control based theory

pulses of  $0.5 \mu\text{s}$  length steps to tackle off resonant errors described by  $-1 < f < 1$ , power variations up to  $\pm 40\%$  and at a Rabi frequency of  $\Omega = 2\pi \times 10 \text{ kHz}$  with 645 steps for a  $\pi/2$  pulse and 445 and 835 steps for  $\pi$  pulses. The three columns shown describe the time line ( $\mu\text{s}$ ), amplitude of the pulse (as a %) and the phase (in degrees). For more information on EPAPS, see <http://www.aip.org/pubservs/epaps.html>